JACC: BASIC TO TRANSLATIONAL SCIENCE VOL. 11, NO. 1, 2026

ORIGINAL RESEARCH - PRECLINICAL

Myosin Modulator Aficamten Inhibits Force by Altering Myosin's Biochemical Activity Without Changing Thick Filament Structure

Saffie Mohran, PhD,[a,b,c,d,*] Kristina B. Kooiker, PhD,[a,b,c,d,*] Ateeqa Naim, BS,[e] Matvey Pilagov, BS,[e] Anthony Asencio, BS,[a,b,d,f] Kyrah L. Turner, BS,[g] Weikang Ma, PhD,[h,i] Galina Flint, MD.,[b,c,d,f] Siyao Jiang, BS,[j] Jing Zhao, BS,[j] Timothy S. McMillen, PhD,[b,d,k] Christian Mandrycky, PhD,[b,d,e] Max Mahoney-Schaefer, BS,[a,b] Thomas C. Irving, PhD,[i] Bertrand C.W. Tanner, PhD,[l] Neil M. Kad, PhD,[e] Michael Regnier, PhD,[b,c,d,f,m] Farid Moussavi-Harami, MD[a,b,c,d,n]

VISUAL ABSTRACT

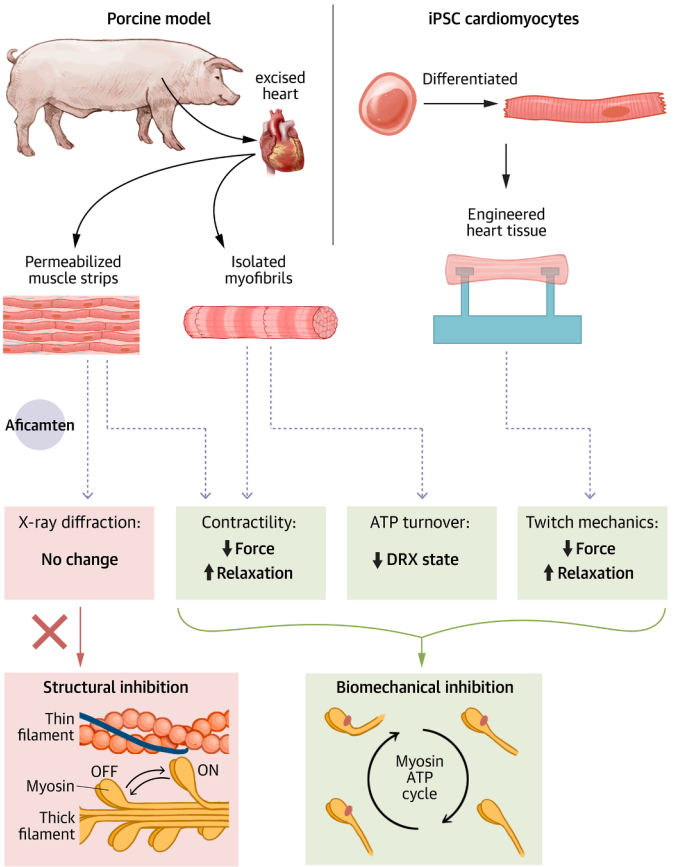

Mohran S, et al. JACC Basic Transl Sci. 2026;11(1):101449.

HIGHLIGHTS

- **Aficamten does not structurally sequester myosin heads along the thick filament.**
- **Aficamten inhibits ATPase activity by modulating myosin heads into slower ATPase state(s), with the emergence of a super slow biochemical nucleotide turnover state.**
- **Aficamten decreases force and calcium sensitivity without altering cross-bridge cycling. Both aficamten and mavacamten inhibit force at the myofibril level while accelerating the relaxation rate.**
- **Although mavacamten and aficamten inhibit cardiac twitch forces, mavacamten reduces the activation kinetics while both accelerate relaxation.**

ISSN 2452-302X https://doi.org/10.1016/j.jacbts.2025.101449

ABBREVIATIONS AND ACRONYMS

Afi = aficamten

HCM = hypertrophic cardiomyopathy

Mava = mavacamten

pCa = negative log of calcium concentration

P_i = inorganic phosphate

SL = sarcomere length

SUMMARY

We investigated the effects of aficamten on cardiac muscle structure, biochemical activity, and contractile function. Aficamten does not structurally sequester myosin heads along the thick filament. It inhibits ATPase activity by decreasing myosin ATPase cycling kinetics, with the emergence of a super slow biochemical nucleotide turnover. This results in decreased force and calcium sensitivity without altering cross-bridge cycling. Our myofibril mechanical assay showed inhibition of force with accelerated relaxation. In engineered heart tissues, while mavacamten and aficamten inhibit cardiac twitch forces, mavacamten reduces the activation kinetics while both accelerate relaxation. (JACC Basic Transl Sci. 2026;11:101449)

Hypertrophic cardiomyopathy (HCM), the most common genetic heart disease with prevalence of around 1:500, is defined by left ventricular (LV) hypertrophy that is not attributed to hypertrophy from another cardiac, metabolic, or systemic process. It can be accompanied by hyperdynamic contraction, outflow tract obstruction, and impaired ventricular relaxation.[1] A genetic cause is identified in about 30% to 60% of patients diagnosed with HCM, and variants in genes encoding for sarcomeric proteins are among the leading causes.[2] Mavacamten (Mava) was recently approved for use in patients with obstructive HCM because it improved exercise capacity and LV outflow tract obstruction.[3,4] Mava selectively binds to myosin and inhibits cardiomyocyte (CM) contractility.[5,6] Studies into the mechanism of Mava have demonstrated that it decreases the rate of inorganic phosphate (Pi) release and stabilizes the OFF state of myosin on the thick filament.[7-10] In addition to Mava, a second small molecule myosin inhibitor, aficamten (Afi), recently completed a phase 3 clinical trial that showed improvement in symptoms and functional capacity in patients with obstructive HCM.[11]

Despite being discovered using a similar myofibril ATPase assay, Afi has a distinct binding site and mechanism of action that differs from Mava. A recent study showed that Afi and blebbistatin share a common binding site on cardiac myosin that is distinct from Mava.[12] The study used saturating concentrations in biochemical assays to investigate how Afi impacts myosin function. Their key conclusions suggest that Afi reduces the rate of actin-activated Pi release and modestly decreases actin-activated ADP release from cardiac myosin S1. They also suggest that Afi stabilizes the weak pre-powerstroke conformation (ADP.Pi), resulting in a loss of force bearing myosin heads and a reduction in contractility.

Here, we provide a comprehensive mechanistic study on how Afi affects the structural, biochemical, and contractile function of myosin within the native sarcomeric structure. By utilizing porcine and human induced pluripotent stem cell (hiPSC) models for our assays, we observe how Afi affects cardiac β-myosin

From the [a]Division of Cardiology, Medicine, University of Washington, Seattle Washington, USA; [b]Center of Translational Muscle Research, University of Washington, Seattle, Washington, USA; [c]Center for Cardiovascular Biology, University of Washington, Seattle, Washington, USA; [d]Institute for Stem Cell and Regenerative Medicine, University of Washington, Seattle, Washington, USA; [e]School of Natural Sciences, University of Kent, Canterbury, United Kingdom; [f]Department of Bioengineering, University of Washington, Seattle, Washington, USA; [g]School of Molecular Biosciences, Washington State University, Seattle, Washington, USA; [h]Department of Biology, Illinois Institute of Technology, Chicago, Illinois, USA; [i]Center for Synchrotron Radiation Research and Instrumentation, Illinois Institute of Technology, Chicago, Illinois, USA; [j]College of Basic Medical Sciences, Dalian Medical University, Dalian, Liaoning, China; [k]Department of Anesthesiology and Pain Medicine, University of Washington, Seattle, Washington, USA; [l]Department of Integrative Physiology and Neuroscience, Washington State University, Seattle, Washington, USA; [m]Department of Neurobiology and Biophysics, University of Washington, Seattle, Washington, USA; and the [n]Department of Laboratory Medicine and Pathology, University of Washington, Seattle, Washington, USA. *These authors contributed equally to this work.

The authors attest they are in compliance with human studies committees and animal welfare regulations of the authors' institutions and Food and Drug Administration guidelines, including patient consent where appropriate. For more information, visit the Author Center.

Manuscript received May 24, 2025; revised manuscript received November 10, 2025, accepted November 13, 2025.

cross-bridge recruitment and cycling under physiological conditions.

METHODS

The data that support the findings of this study are available from the corresponding author upon reasonable request.

ANIMAL USE AND ETHICS. All experiments followed protocols approved by both the University of Washington and the Illinois Institute of Technology Institutional Animal Care and Use Committees according to the "Guide for the Care and Use of Laboratory Animals" (National Research Council, 2011). Muscle tissue was collected in accordance with the United Kingdom Animals (Scientific Procedures) Act 1986 and associated guidelines. Farm pig hearts or Yucatan mini pigs (Exemplar Genetics) were obtained immediately after the animal was sacrificed and rinsed in cold oxygenated Tyrode's buffer.

MYOFIBRIL SINGLE-MOLECULE IMAGING OF ATP TURNOVER. Myofibril isolation and flowcell preparation can be found in the Supplemental Methods. Flowcells were prepared as described previously[13] and connected at one end to a syringe pump (WPI, AL-1000) and at the other to a 1.5-mL microcentrifuge tube with holes to allow access of pipette tips. 200 μL of prepared porcine myofibril suspension (Supplemental Methods) was added to the 1.5-mL microcentrifuge tube and drawn into the flowcell at 1 mL/min then washed back through at 0.2 mL/min. To allow adhesion of myofibrils to the PLL-coated surface, flowcells were incubated on ice for 30 minutes. Excess nonadherent myofibrils were withdrawn from the flowcell using 600 μL Prep buffer (Supplemental Methods) at 10 mL/min.

Myofibrils were incubated with Cy3-ATP buffer (Prep buffer + 1 μmol/L Cy3-ATP, 500 μmol/L ATP, 0.5 mmol/L phosphoenolpyruvate (PEP), 2.2 U Pyruvate kinase) for 30 minutes at room temperature (RT). Where used, aficamten (MedChemExpress, Cat. No: HY-139465) solubilized in 100% dimethyl sulfoxide (DMSO), was added to the Cy3-ATP buffer and Chase buffer (Prep buffer + 5 mmol/L ATP, 5 mmol/L PEP, 22 U Pyruvate kinase) at final concentrations stated in **Figure 1** (final DMSO remained constant at 0.06% v/v). Following this, a single frame was taken of the myofibril fully saturated with Cy3-ATP, followed by a rapid wash with Chase buffer at 10 mL/min. To increase efficiency, flowcells were mounted onto a custom-built automated stage programmed to move between user-specified positions along 1 axis. Between each frame, images from neighboring myofibrils were taken. Use of this automated stage allowed up to 4 myofibrils to be simultaneously imaged during the 30-minute imaging period. Six to 15 myofibrils were measured at each condition then rate constants were binned into fast (0.05-0.005 s^{-1}), slow (0.005-0.0005 s^{-1}), or super slow (< 0.0005 s^{-1}).

All imaging was carried out at RT using a custom-built oblique angle fluorescent microscope.[14] The sample was illuminated for 15 ms every 5 seconds using a 561 nm laser (OBIS LS laser, Coherent) to excite Cy3-ATP, for a total of 30 minutes.[15]

To extract the rate of fluorescence decay for each myofibril, an ROI was drawn using ImageJ to encompass the entire myofibril, and the total intensity profile was extracted over time. These data were transferred to Microsoft Excel and then fitted to a triple exponential decay, providing both rate constant and amplitudes.

X-RAY DIFFRACTION. Wild type Yucatan mini-pig hearts were provided by Exemplar Genetics LLC. Permeabilized tissue preparation and beamline specifications were performed as previously described.[16] X-ray diffraction experiments were performed at the BioCAT beamline 18ID at the Advanced Photon Source, Argonne National Laboratory.[17] Skinned muscle preparations were mounted in a custom rig. The muscle was incubated in a customized chamber with the solution temperature at 28 °C. The sarcomere length (SL) of the muscles was set to 2.3 μm by measuring the diffraction pattern of the fiber utilizing a helium-neon laser (633 nm). X-ray fiber diffraction patterns were collected in pCa 8.0 solution in the absence or presence of 50 μmol/L of Afi. Fibers were incubated for 15 minutes in 50 μmol/L Afi before imaging. Analysis of x-ray diffraction images were done as described previously.[18,19]

DEMEMBRANATED TISSUE MECHANICS. Tissue preparation and solutions are described in the Supplemental Methods.

Isometric force and rate of tension redevelopment. Porcine LV tissue was permeabilized overnight at 4 °C in a 50% glycerol relaxing solution with 1% Triton X-100. Permeabilized LV strips were dissected to ~120 × 600 μm and mounted between a force transducer (Aurora Scientific, model 400A) and a motor (Aurora Scientific, model 315C) using aluminum T-clips (Aurora Scientific).[20] The tissue was stretched to an SL of ~2.3 μm for each experiment. Experiments began in a relaxing solution with pCa (= $-\log_{10}[Ca^{2+}]$) of 8.0, then moved through a pCa curve from 6.0 to 4.5 in physiological solution (pH 7.0) at 21 °C with 3% dextran. Experiments were done in 3 groups of untreated (no drug [ND]),

FIGURE 1 **Increasing Concentration of Afi Results in the Emergence of a Very Slow ATPase State**

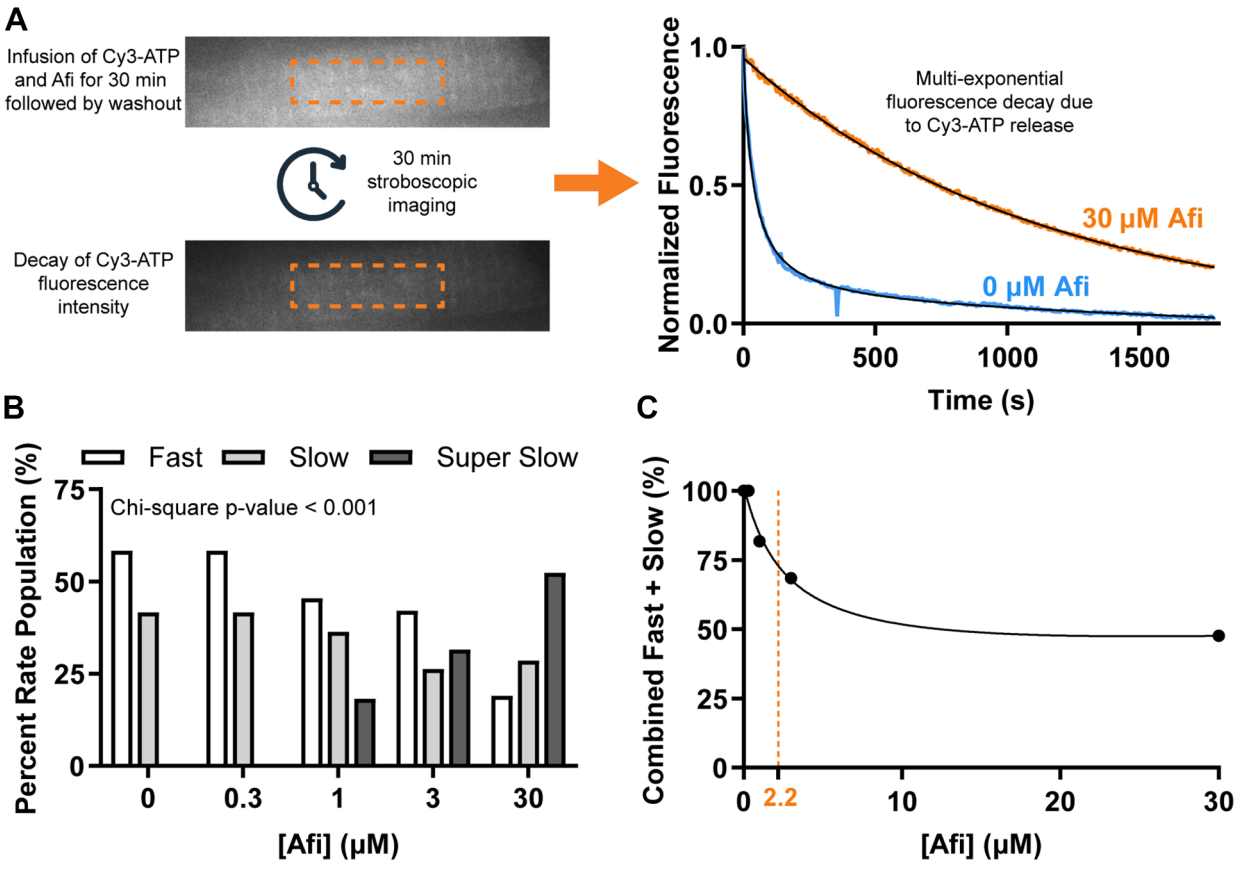

(A) Experimental protocol used, showing region analyzed (in box) for single-molecule ATP imaging (left) and example tracing of normalized fluorescence in absence (blue) or presence (orange) of 30 μmol/L aficamten (Afi) (right). (B) The percentage of all rate constants in the fast, slow, or super slow state at each concentration of Afi shows the emergence of the super slow state at 1 μmol/L Afi and above. The data is presented as the percentage of each rate at each concentration of Afi. Chi-square analysis was used to test for significant changes in the populations across concentrations. (C) To calculate the K_d of 2.21 (± 0.76) μmol/L (orange dashed line), all fast and slow state percentages at each concentration were combined and fit to a weak binding equation (S/[K+S]). 6-15 myofibrils were measured at each concentration of Afi, then rate constants were binned into fast (0.05-0.005 s^{-1}), slow (0.005 – 0.0005 s^{-1}), or super slow (<0.0005 s^{-1}).

1 μmol/L Afi, or 1 μmol/L Mava (MedChemExpress). The tissue was incubated in relaxing conditions with or without compound for 2 hours at RT before experimentation. During experimentation, tissues were allowed to reach stead-state force (F) at each pCa. F-pCa curves were collected with custom code using LabView software version 9.0.1 (National Instruments) and fit to the Hill equation in GraphPad Prism version 10.5.0 (GraphPad Software). The rate of tension redevelopment (k_{TR}) was measured at each pCa with a 15% slack and restretch.

Sinusoidal length-perturbation analysis of viscous modulus. Permeabilized porcine myocardial strips (~180 × 700 μm) were mounted between a piezoelectric motor (P841.40, Physik Instrumente) and a strain gauge (AE801, Kronex) using aluminum T-clips. Each strip was lowered into a 30-μL droplet of relaxing solution (pCa 8.0) maintained at 28 °C. SL was then set to 2.3 μm, and the solution was exchanged with activating solution (pCa 4.8). Sinusoidal length perturbations of 0.125% myocardial strip length (clip-to-clip) were applied at multiple frequencies from 0.125 to 250 Hz to measure the complex modulus as a function of frequency.[21] The complex modulus describes viscoelastic myocardial stiffness which arises from the change in stress (= force per cross-sectional area) divided by the change in muscle length that is in-phase (= elastic modulus) and out-of-phase (= viscous modulus) with the oscillatory length change at each discrete frequency.

The viscous modulus at pCa 4.8 was fit to a polynomial to extract the maxima and minima frequencies for each condition, where the "dip frequency" describes force-generating events and cross-bridge recruitment while the "peak frequency" describes cross-bridge distortion events and cross-bridge detachment rate.[22-24] These characteristic "dip" and "peak" regions of the viscous modulus were used to assess the effects of Afi and Mava on cross-bridge cycling kinetics under maximal Ca^{2+}-activated conditions.

MYOFIBRIL MECHANICS. Myofibril activation and relaxation measurements were performed on a custom setup as previously described.[25,26] Myofibrils were isolated from LV porcine tissue using a tissue homogenizer for 10 seconds. Myofibrils were then plated onto the custom setup and were mounted between a glass force transducer and an inflexible motor arm. A dual photodiode system measured myofibril force by recording needle deflection. The force transducer needle stiffness measured 7.98 μm/μN. A double-barreled glass pipette delivered relaxing (pCa = 8.0) and activating (4.5) solutions to the isolated myofibril using a rapid switching technique. Activation and relaxation data were collected at 21 °C and fitted as previously described.[26]

hiPSC DIFFERENTIATION AND ENGINEERED HEART TISSUE CASTING. Differentiation of WTC11 hiPSCs into CMs is detailed in the Supplemental Methods. To cast hiPSC-CMs into engineered heart tissues (EHTs), 500,000 21-day-old lactate-purified WTC11 hiPSC-CMs were mixed with 50,000 HS27a (human marrow stromal cells[27]), 5 mg/mL fibrinogen (Sigma), and 3 unit/mL thrombin (Sigma) then cast onto wells with PDMS postarrays.[28] Gelation occurred over the following 1.5 hours, then tissues were moved to a fresh 24-well plate with RPMI + B27 + insulin + 5 g/L aminocaproic acid (Sigma) and stored at 37 °C. Media was changed every 2 to 3 days while the tissue compacted and matured.

INTACT TWITCH ASSAY. EHTs were cut off posts 2 weeks after casting (35 days postinducement of cardiomyocyte differentiation) and moved into a dish containing DMEM/F12 (Gibco) continuously bubbled with 95% O_2/5% CO_2 to maintain physiological pH and mounted between 2 platinum omega clips. The EHT was then mounted into the Intact Muscle Chamber System (IonOptix) and perfused with DMEM/F12 supplemented with $CaCl_2$ (final Ca^{2+} = 1.8 mmol/L) continuously bubbled with 95% O_2/5% CO_2. EHTs were electrically paced at 1 Hz, maintained at ~32 °C and allowed to contract isometrically throughout the experiment. EHTs were given 15 minutes to stabilize, during which time optimal length was set to where the total amplitude of the twitch no longer increased. Drug titrations were performed with 0.01% DMSO (ND), then 1 and 2 μmol/L Afi or 0.5 and 1 μmol/L Mava with 15 minutes incubations at each concentration. For each condition, 30-second traces were recorded and analyzed using IonWizard software (IonOptix).

STATISTICAL ANALYSIS. We used GraphPad Prism version 10.5.0 (GraphPad Software) for data presentation and statistical analysis unless otherwise stated. The data are presented as mean ± SEM. All data was tested for normality using the D'Agostino and Pearson test, except for the EHT parameters, which used the Shapiro-Wilk test because of lower n values. For porcine isometric permeabilized tissue mechanics and myofibrils, we used an ordinary 1-way analysis of variance with Tukey's post hoc test for multiple pairwise comparisons. For viscous modulus measurements, IBM SPSS Statistics version 29.0.1.0 (171) was used. Nested linear mixed-effect models were utilized for the minimum or maximum frequency parameters determined from polynomial curves fit from the viscous modulus. Treatment was considered the fixed effect with biological replicate (pig) as the random effect in which technical replicates were nested. Post-hoc analysis used the Fisher least significant difference test. For x-ray diffraction and EHT twitch analysis, we used paired 2-tailed Student's *t*-tests. For in vitro motility, we used 2-way analysis of variance with Šídák's post hoc test. A P value <0.05 was considered statistically significant.

RESULTS

AFI INHIBITS ATPase ACTIVITY WITHOUT STRUCTURALLY SEQUESTERING MYOSIN HEADS ON THE THICK FILAMENT. To understand the effect of Afi on ATPase activity, we assessed the decay of fluorescently labeled ATP (Cy3-ATP) in permeabilized porcine cardiac myofibrils as myosin cycles and releases Cy3-ADP (**Figure 1A**). Experiments were performed on relaxed myofibrils after infusion with Cy3-ATP and Afi at concentrations ranging from 0 to 30 μmol/L for 30 minutes. This was followed by a wash-out of Cy3-ATP with unlabeled ATP (with Afi) and 30 minutes of stroboscopic imaging to image the decay in fluorescence intensity. The intensity was then fit to a multiexponential decay to extract multiple rate constants and their relative amplitudes (**Figure 1A**). For each myofibril, the resultant rate constants were classified as 1 of 3 ATP

FIGURE 2 **50 μmol/L Afi Minimally Affects Thick Filament Structure in Relaxed Porcine Tissue**

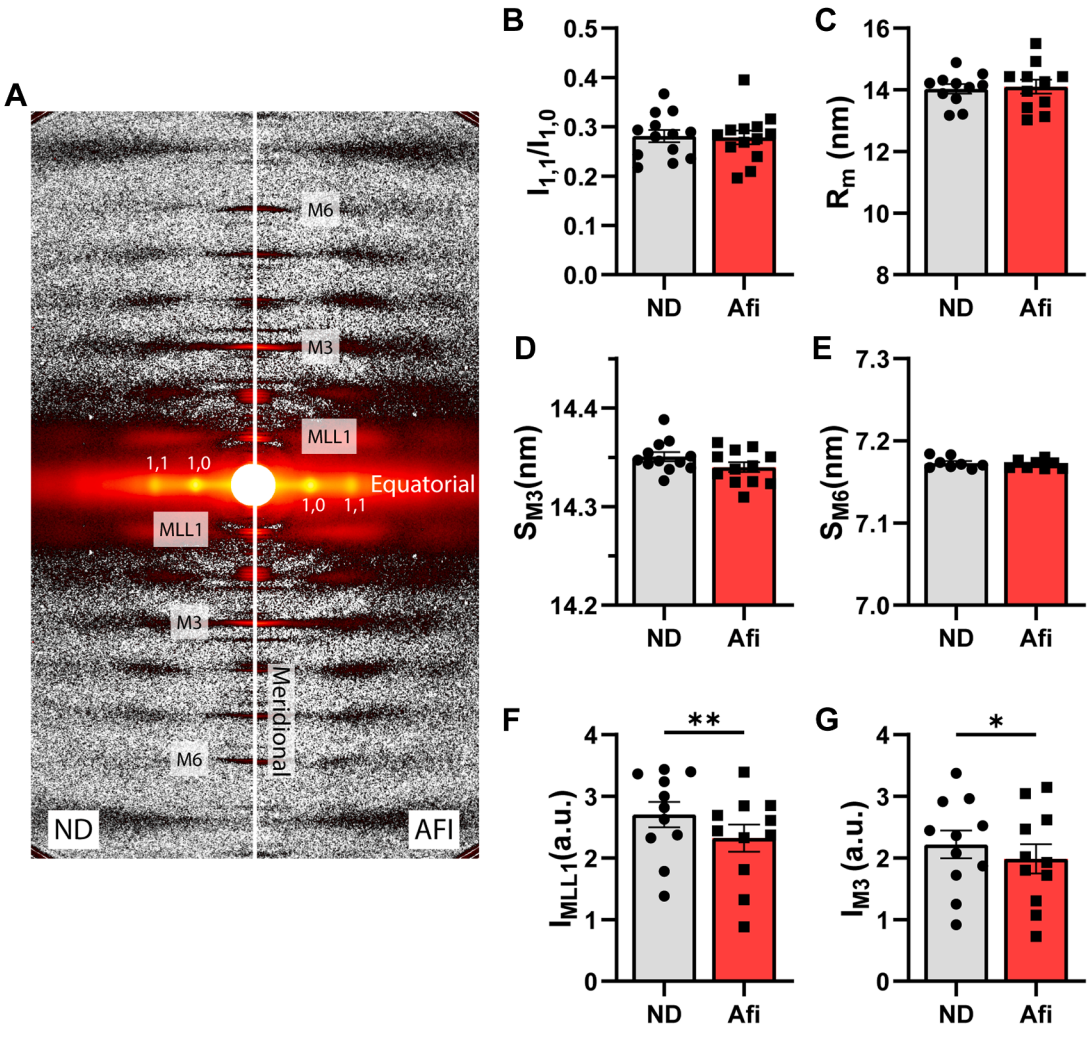

(A) Representative x-ray diffraction patterns before (no drug [ND]; left) and after (aficamten [Afi]; right) incubation in 50 μmol/L Afi. Afi does not affect the (B) intensity ratio ($I_{1,1}/I_{1,0}$) or the (C) radius of the cross-bridge center of mass (R_m), suggesting that myosin heads are not moving toward or away from the thick filament backbone because of Afi. The spacing of the (D) third-order of myosin-based reflection (S_{M3}) and (E) sixth-order of myosin-based reflection (S_{M6}) are not changed. The intensity of the (F) third-order myosin-based reflection (I_{M3}) and (G) first-order myosin-based layer line (I_{MLL1}) slightly decrease after Afi incubation, suggesting that Afi causes some disorder in the myosin heads. N = 13 tissues samples were prepared and measured. Paired Student's *t*-tests were performed for each measurement. All data is presented as mean ± SEM. *$P < 0.05$, **$P < 0.01$, ***$P < 0.001$.

turnover states (fast, slow, super slow). **Figure 1B** and Supplemental Figure S1 show that as the concentration of Afi increases, the population of myosin heads in the fast state decreases, with the emergence of a super slow state at 1 μmol/L Afi. Interestingly, the population in the slow state seems to only minimally decrease with increasing Afi. To plot a binding isotherm for Afi, we combined the fast and slow states, which represents myosin heads not in the super slow ATPase state, and fit a weak binding equation (S/[K+S]) to calculate a K_d of 2.21 ± 0.76 μmol/L (**Figure 1C**). This is in the same range as was seen by Hartman et al.[29]

In addition to assessing the biochemical inhibition of myosin ATPase activity by Afi we utilized small angle x-ray diffraction to assess the impact on thick filament structure. Previous studies have shown that myosin modulators can significantly affect the

position of myosin and the organization of the thick filament structure.[16,19] Paired x-ray diffraction images were collected under relaxed conditions (pCa 8.0) with ND and in the presence of 50 μmol/L Afi (**Figure 2A**, Supplemental Table 1). Measures of the equatorial reflections showed no significant difference in the lattice spacing ($d_{1,0}$) (Supplemental Figure S2) or intensity ratio ($I_{1,1}/I_{1,0}$) (**Figure 2B**). Quantification of the radius of the center of mass of the myosin heads (R_m) (**Figure 2C**), which describes the average distance of the myosin heads from the thick filament, also showed no significant difference in the presence of Afi. These results show that in saturating conditions, Afi does not induce changes to the sarcomere interfilament spacing or the position of the myosin heads relative to the thick and thin filaments. Additional assessment of the axial spacing from the third-order myosin-based meridional reflection (S_{M3}) (**Figure 2D**) and the sixth-order myosin-based meridional reflection (S_{M6}) (**Figure 2E**) showed no change in the presence of Afi. These spacing measurements indicate that Afi does not induce any structural change in position between the myosin crowns (S_{M3}) or alter the thick filament backbone (S_{M6}) in a manner typically associated with strain and mechano-sensing.

Interesting, both the intensity of the first-order myosin-based layer line (I_{MLL1}) (**Figure 2F**) and third-order myosin based meridional reflection (I_{M3}) (**Figure 2G**) in the presence of Afi decreased by 10.5% compared with ND paired controls. The decrease in I_{MLL1} and I_{M3} describes a reduction in the number of quasi-helically ordered myosin heads on the thick filament.

Both the equatorial and meridional results with Afi are different from those described by Anderson et al and Ma et al (Supplemental Table 2) for Mava.[7,19] They reported that Mava significantly shifts the radial position of myosin toward the thick filament backbone and increases the helical ordering of the myosin crowns. These structural modulations caused by Mava, coupled with the ATPase inhibition, result in significantly inhibited actomyosin interaction and sarcomeric contractility.

AFI INHIBITS CONTRACTILE FORCE WITHOUT ALTERING CROSSBRIDGE CYCLING KINETICS IN PERMEABILIZED PORCINE TISSUE. To assess how the biochemical and structural effects of Afi affected cardiac contractility, we first examined steady-state force production, calcium sensitivity, and myosin cycling kinetics in permeabilized porcine tissue. **Figure 3A** shows the concentration dependence of the time required to reach steady state inhibition by Afi. At higher Afi concentrations, such as those used for the ATP turnover (**Figure 1**) and x-ray diffraction (**Figure 2**) experiments, force is fully inhibited after 10 minutes. To perform functional measurements of contractility, the remaining steady-state force measurements were performed at sarcomere length of 2.3 μm after a 2-hour incubation either in the absence of drug (ND; 0.1% DMSO) or in the presence of 1 μmol/L Afi or Mava. Afi and Mava had similar inhibitory effects for isometric contraction measurements (**Figures 3B to 3F**). Both drugs shifted the force-pCa relationship to the right (**Figure 3B**), with significantly decreased maximal calcium activated force (**Figure 3C**) and calcium sensitivity of force (pCa_{50}) (**Figure 3D**). There were no changes in the Hill coefficient (**Figure 3E**), suggesting no changes in cooperativity of contractile activation. There were also no changes in cross bridge cycling kinetics as determined by the rate of tension redevelopment (k_{TR}) (**Figure 3F**).

Viscous modulus was measured in maximally activating conditions sweeping frequencies from 0.125 to 100 Hz to assess steady state crossbridge attachment and detachment. The overall magnitude of the viscous modulus decreased (**Figure 3G**), which is consistent with a decrease in the number of strongly bound cross bridges. The horizontal positions of the minimum and maximum frequencies indicate differences in cross bridge kinetics caused by cross bridge attachment and detachment rates, respectively. The dip in the modulus-frequency relationship (minimum viscous modulus) was shifted toward a lower frequency for Mava but not Afi (**Figure 3H**), suggesting that the rate of crossbridge attachment decreased only for Mava. No frequency shifts were observed for the peak viscous modulus values (**Figure 3I**), indicating no change in rate of crossbridge detachment.

AFI INHIBITS FORCE GENERATION AND ACCELERATES RELAXATION KINETICS IN ISOLATED MYOFIBRIL PREPARATIONS. The utilization of subcellular myofibril preparations allows for the measurement of force and kinetics during the transition states between activation and relaxation. To switch the myofibril between maximal activation (pCa 4.5) and relaxation (pCa 8.0) solutions we utilize a rapid solution switching method with a double-barreled pipet. Representative traces in **Figure 4A** show the normalized force relationship during myofibril activation and relaxation in the presence of ND, 1.0 μmol/L Afi, or 0.5 μmol/L Mava.

Switching between pCa 8.0 and pCa 4.5 did not significantly affect the exponential rate (k_{ACT}) of

FIGURE 3 Afi and Mava Inhibit Force, Calcium Sensitivity, and Viscous Modulus Dip Frequency in Demembranated Tissue Mechanics

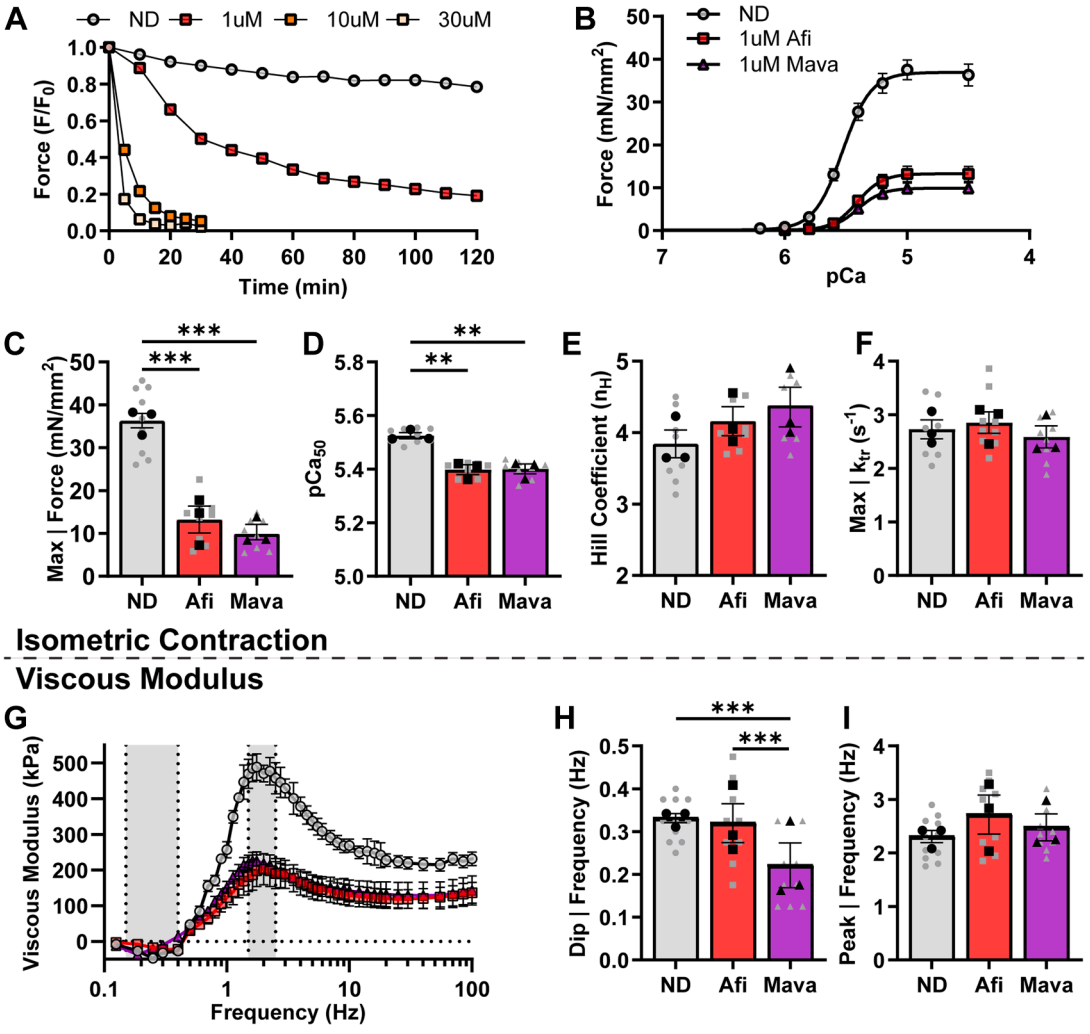

(A) The time required for full force inhibition by Afi decreased as the concentration of Afi increased. After 2-hour incubation in ND, 1 μmol/L Afi, or 1 μmol/L mavacamten (Mava), (B) the force-pCa relationships were shifted rightward for both drugs because of decreases in (C) maximal calcium-activated force and (D) calcium sensitivity. (E) The Hill coefficient and (F) maximal calcium-activated rate constant of tension redevelopment (k_{tr}) were not affected. (G) Viscous moduli values were plotted against frequency to assess cross-bridge binding and kinetics. At maximal activation, both drugs decreased moduli values across much of the frequency range (H) The dip frequency (minimum viscous modulus) and (I) peak frequency (maximum viscous modulus) were not affected by Afi, but the dip frequency was shifted lower for Mava suggesting slower cross-bridge attachment rate. 8-11 tissues samples from 3 different pigs were prepared and measured for each condition. 1-way analysis of variance with Tukey's post hoc test was used for isometric tension analyses. For viscous modulus, nested linear mixed-effect models were utilized with post hoc Fisher least significant difference test. All data is presented as mean ± SEM. *$P < 0.05$, **$P < 0.01$, ***$P < 0.001$. Abbreviations as in Figure 2.

force generation in the presence of either Afi or Mava (1.10 ± 0.02 and 0.79 ± 0.08 s^{-1}) compared with untreated controls (1.01 ± 0.08 s^{-1}) (Figure 4C). Interestingly, however, Afi and Mava results were significantly different ($P = 0.033$) from each other, where Afi was slightly but not significantly elevated and Mava was slightly reduced. In addition to the activation kinetics, we observed that both Afi and Mava significantly inhibited the maximally activated force (37.6 ± 2.8 and 37.5 ± 2.9 nN/μm^2) of the isolated porcine cardiac myofibrils compared with untreated controls (76.7 ± 3.0 nN/μm^2) (Figure 4B).

Upon the rapid transition from activating to relaxing solution, we observed a biphasic relaxation

FIGURE 4 **Afi and Mava Inhibit Maximal Calcium-Activated Force and Slow Relaxation Kinetics in Isolated Myofibrils**

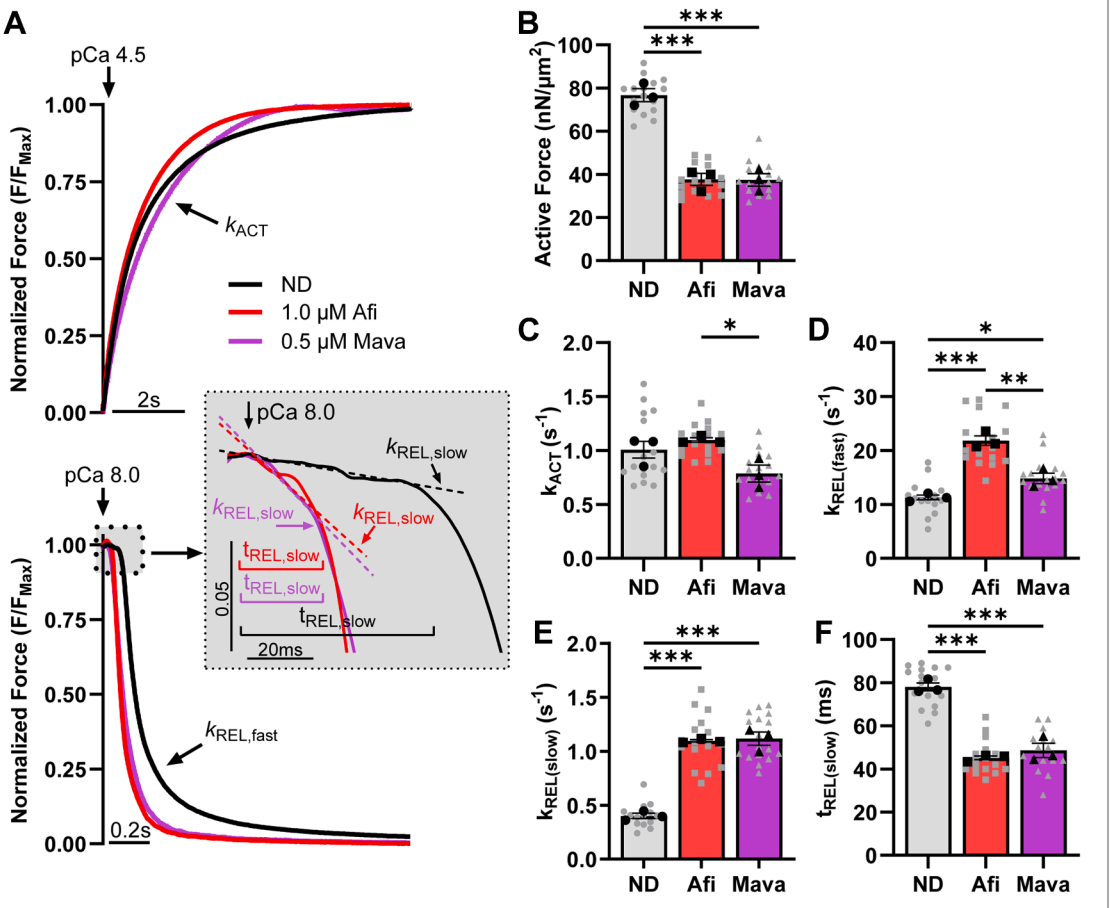

(A) Average traces showing activation (top), the fast phase of relaxation (bottom), and the slow phase of relaxation (inset). (B) Both Afi and Mava inhibited maximal calcium-activated force. (C) Neither drug changed the rate constant of activation (k_{ACT}) vs ND. However, Afi and Mava were significantly different from each other. (D) The rate constant of the fast phase of relaxation ($k_{REL\ (fast)}$) and (E) the rate constant of the slow phase of relaxation ($k_{REL\ (slow)}$) were increased for both drugs vs ND, and (F) the time of slow relaxation ($t_{REL\ (slow)}$) was shorter for both drugs vs ND. N = 16-17 myofibrils from 3 different pigs were prepared and measured for each condition. 1-way analysis of variance with Tukey's post hoc test was used for analysis. All data is presented as mean ± SEM. *$P < 0.05$, **$P < 0.01$, ***$P < 0.001$. Abbreviations as in Figures 2 and 3.

relationship that consists of both an initial linear "slow phase" and exponential "fast phase" of relaxation as the force returns to baseline. The linear rate constant from the slow phase of relaxation ($k_{REL,slow}$) describes the rate of cross-bridge detachment.[30] Previous studies have shown this rate constant value is independent of the Ca^{2+} dissociation from troponin.[31] The duration of the slow phase ($t_{REL,slow}$), however, depends on the time of thin filament deactivation which is dependent on the properties of thin filament regulatory proteins (troponin and tropomyosin) and the calcium concentration during activation. The final component of myofibril relaxation is the exponential rate constant ($k_{REL,fast}$) that measures the rapid return of force to baseline. This measurement characterizes multiple different intersarcomere dynamics and involves both active and passive properties that enable the sarcomeres to relax.[31]

Afi significantly accelerated $k_{REL,fast}$ (21.9 ± 0.9 s^{-1}) compared with Mava (14.8 ± 1.0 s^{-1}) and to ND (11.3 ± 0.4 s^{-1}) (Figure 4D). Both Afi and Mava significantly increased $k_{REL,slow}$ (1.10 ± 0.01 and 1.12 ± 0.06 s^{-1}) compared with ND (0.40 ± 0.03 s^{-1}) (Figure 4E). Both compounds also significantly decrease $t_{REL,slow}$ (45.1 ± 0.9 and 48.6 ± 3.3 ms) compared with ND (78.1 ± 1.8 ms) (Figure 4F). These significant effects of Afi on myofibril relaxation kinetics were very

FIGURE 5 Afi and Mava Decrease Tension Index in a Concentration-Dependent Manner Primarily Through Changes in Peak Tension in Engineered Heart Tissues

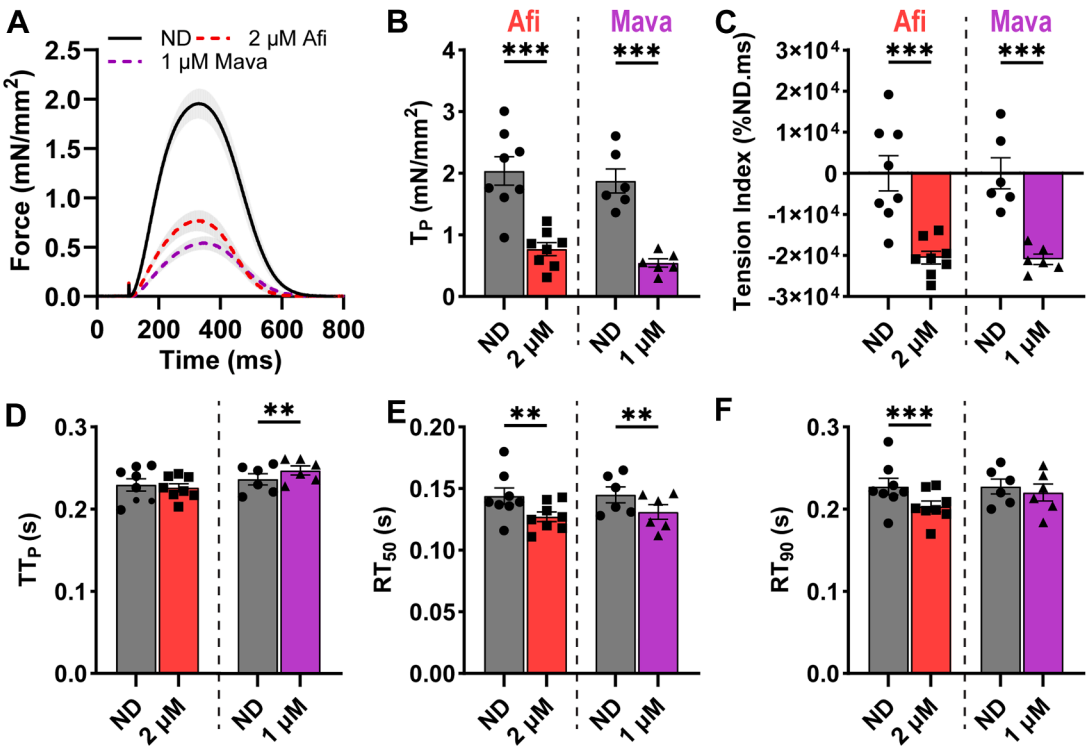

(A) Average twitch traces of paired experiments (ND vs Afi or ND vs Mava) were normalized to EHT cross-sectional area. (B) Peak twitch tension was inhibited by both Afi and Mava leading to (C) negative tension index values for both drugs. (D) Time to peak tension (TT_P) was longer for Mava but not Afi. (E) Time to 50% relaxation (RT_{50}) was shorter for both Afi and Mava, and (F) time to 90% relaxation (RT_{90}) was only shorter for Afi. 6-8 EHTs were matured and measured. Paired Student's *t*-tests were performed for each EHT. All data is presented as mean ± SEM. *$P < 0.05$, **$P < 0.01$, ***$P < 0.001$. Abbreviations as in Figures 2 and 3.

interesting given the lack of differences in k_{TR} or viscous modulus frequencies.

AFI DECREASED THE TENSION TIME INTEGRAL PRIMARILY THROUGH INHIBITION IN FORCE PRODUCTION IN INTACT EHTs. To determine how all the reductionist preparation results integrate to alter physiological contractile function, we compared how Afi and Mava impact twitch tension and kinetics in intact EHTs made from hiPSC-CMs. At 21 days post differentiation, hiPSC-CMs were cast onto PDMS posts along with stromal cells in a fibrin gel and then allowed to compact and mature for 2 weeks. On day 14 postcasting, EHTs were cut from the posts, secured between 2 platinum omega clips, and mounted between a force transducer and motor arm. Average twitch tension normalized to ND (0.01% DMSO) was inhibited in the presence of Afi and Mava (Figure 5A and Supplemental Table S3), although higher concentrations of Afi (2 μmol/L) were required to reach similar levels of inhibition compared with Mava (1 μmmol/L) (Figure 5B). The substantial decreases in force led to negative tension index values (Figure 5C), which has been shown to be predictive of hypocontractility at the whole-organ level.[20,32] Time to peak tension (TT_P) (Figure 5D) was significantly longer for Mava but not changed for Afi. Time to 50% relaxation (RT_{50}) (Figure 5E) and time to 90% relaxation (RT_{90}) (Figure 5F) were significantly shorter for Afi, while only RT_{50} was shorter for Mava.

DISCUSSION

In this study, we investigated the biophysical and biochemical mechanisms underlying the ability of

aficamten (Afi) to reduce cardiac contractility. Afi, a second-in-class, myosin-specific small molecule in phase 3 clinical trials, has demonstrated functional improvements comparable to the FDA-approved mavacamten (Mava) in patients with obstructive HCM.[11,33] Recent findings by Hartman et al[29] revealed that Afi significantly inhibits Pi release and may reduce ADP release rate constants in purified myosin S1 in unloaded conditions, consistent with pre-powerstroke (M.ADP.Pi) modeling. Building on these findings, we explored how Afi modulates myosin structural organization and sarcomeric contractility under load at myofibril and tissue levels.

Using a porcine cardiac model that expresses β-myosin, we found that Afi significantly reduces the number of myosin heads available to interact with actin and produce force. Interestingly, there was an increased population of low ATPase activity myosin and emergence of a super slow ATPase activity population with increasing Afi in the absence of the structural changes monitored by x-ray diffraction. This suggests that impaired ATPase activity can be achieved without structural sequestration. Our results also suggest Afi induces significant acceleration of relaxation kinetics in conditions of permeabilized myofibrils and intact EHTs. By first utilizing the myofibril platform, the significant acceleration in relaxation kinetics can be attributed to direct modulation of the sarcomere as we isolate crossbridge cycling kinetics by controlling the exposure duration and concentration of Ca^{2+} to the thin filament. Transitioning into EHTs, we still observe accelerated relaxation that transcends the increased system complexity by introducing both myofibril and non-myofibril components of cellular regulation including Ca^{2+} handing and multiple levels of compliance within the tissue.

THE POOL OF RECRUITABLE MYOSIN CAN BE AFFECTED BY BIOCHEMICAL AND/OR STRUCTURAL MODULATION. The biochemical ATPase states (SRX and DRX) and thick filament structure (ON and OFF) have often been thought to be interchangeable. However, recent studies have provided strong evidence suggesting that these biochemical and structural measurements are uncoupled under different conditions.[34,35] Structural assessments of Mava bound to β-myosin have shown that it increases the formation of head-to-head and head-to-tail complexes in the thick filament.[36,37] These alterations to the myosin head structure caused by increased affinity of inorganic phosphate to myosin (M.ADP.Pi) lead to increased myosin crown organization along the thick filament backbone that can be measured by structural imaging techniques such as x-ray diffraction[19] and cryo-em.[36] The induced head-head structural interaction also increases the inhibitory effect of Mava as shown by the significant decrease in K_i between isolated β-myosin S1 and HMM protein preparations (K_i, 1.76 and 0.32 μmol/L, respectively).[34]

In contrast to Mava, Afi does not induce changes in the myosin crown organization or position with respect to the thick filament, suggesting that Afi achieves ATPase inhibition through alternative mechanisms. Molecular modeling and compound competition experiments[12] show that Afi binds in the same region of myosin as blebbistatin and requires the same M.ATP → M.ADP.Pi transition state to bind.[38] This binding state complicates performing reductionistic assays to assess actomyosin affinity and ADP release kinetics as these require rigor (A.M.) conditions before mixing with nucleotide. Utilization of the modified Cy3-ATP nucleotide replacement assay enabled us to introduce Afi to myosin in the presence of ATP, allowing the compound to bind before performing nucleotide replacement assays. This technique allows us to perform compound titration curves and validate the emergence of the super slow state, a compound induced nucleotide replacement rate 10× slower than the described 0.002 s^{-1} SRX state observed with saturating 30 μmol/L Mava utilizing the same technique.[15] This inhibited population increased in prevalence at greater compound concentrations and maintained a saturating rate constant value of constant value of ~0.0002 s^{-1}, consistent with the rate constant observed in high concentrations of Afi by Hartman et al.[29] They also found that Afi binds between the upper and lower 50 kDa domains of myosin, same as the blebbistatin binding pocket.[12] This could explain how a similar slowing of ATP turnover occurred in the presence of high concentrations of blebbistatin.[37] This was attributed to the stabilization of switch 2 in myosin heads to limit phosphate release.[39] Future studies could determine if a similar mechanism occurs with Afi. Overall, these results show that Afi causes greater inhibition of the enzymatic activity of myosin compared with Mava[37] without inducing large-scale changes in myosin crown organization or positions relative to the thick filament backbone.

STUDY LIMITATIONS. One limitation of the Cy3-ATP experiments was the inability to perform the myofibril biochemical assessments under load. The current system does not allow for the myofibrils to be lifted and cannot be stretched to longer sarcomere lengths such as the 2.3-μm sarcomere length that was

utilized for the x-ray diffraction and contractility experiments. Few publications have performed biochemical ATP turnover experiments utilizing permeabilized CMs. Future work in our group aims to address this limitation and better understand how stretch can impact myofibril nucleotide cycling kinetics.

BIOCHEMICAL INHIBITION DOES NOT SIGNIFICANTLY AFFECT THE CROSSBRIDGE KINETICS OF MYOSIN HEADS ACTIVELY CYCLING DURING CONTRACTION. Unregulated in vitro motility results suggest that Afi reduces the number of myosin heads available to interact with actin without incurring significant drag associated with a decrease in fraction moving (Supplemental Figure S3, matching results by Hartman et al[29]). In our steady-state and dynamic contractility experiments, this reduction in available myosin resulted in inhibited force generation. Steady state permeabilized fiber experiments yield no significant differences in cooperative activation (n_H), myosin cycling kinetics during tension re-stretch (k_{TR}), or viscous modulus (myosin attachment and detachment frequencies) at the experimental 2.3-μm sarcomere length. Interestingly, myofibril contractile kinetics show that Afi significantly decreases the duration of thin filament deactivation ($t_{REL,slow}$) and accelerated both the slow and fast phases of relaxation of maximally activated myofibrils back to resting baseline. These significant changes in relaxation kinetics are interesting caused by the lack of change in myosin cycling kinetics observed in steady state k_{TR} and viscoelastic measurements, which suggest no significant changes in the load-dependent ADP release rate of myosin heads that are actively cycling and interacting with actin. With Afi inducing significant changes to relaxation kinetics, we hypothesize that the accelerated relaxation kinetics observed in the myofibrils are induced by a reduced pool of actively interacting myosin heads with actin during the transition from high to low calcium solutions.

IMPLICATIONS OF MODULATING CONTRACTILITY THROUGH BIOCHEMICAL AND STRUCTURAL INHIBITION. By biochemical inhibition, Afi decreases the pool of myosin heads that can interact with actin, reducing the capacity of contractility without structurally sequestering heads along the thick filament backbone. Unlike Mava, this mechanistic pathway preserves the recruitment of myosin heads to actin during activation as illustrated by the lack of significant changes in the steady-state fiber viscous modulus dip-frequency, steady state k_{TR}, the myofibril k_{ACT} rate constant values, and the TT_p EHT assessment. These differences, however, raise questions regarding how the biochemical and structural modulation of myosin may impact the ability to recruit myosin under varying external conditions. As presented by Ma et al,[40] the structural and functional cardiac relationships to inotropic interventions like Ca^{2+}, increased chronotropy, length-dependent activation, and β-adrenergic stimulation are persevere in the presence of Mava. These significant findings help describe how Mava increased maximum exercise capacity in patients with obstructive HCM[41] and a subset of nonobstructive HCM patients.[42] In future studies, it will be important to see how the biochemical inhibition of Afi affects cardiac reserve and if the compound can preserve these relationships like Mava.

CONCLUSIONS

Our study shows that the main mechanism of Afi inhibition is through inhibition of myosin S1 head activity that reduces the number of myosin heads that bind and cycle during contraction. This reduction on recruitable myosin is achieved without the structural sequestration of the myosin heads on the thick filament backbone, a significant difference to the mechanistic pathway described for Mava. This finding distinctly decouples the association of biochemical SRX state from the structural ON/OFF states as a mechanism for cardiac muscle inhibition. It also confirms the emergence of an even slower rate of ATP turnover as Afi increases in concentration.[29] Afi does not significantly impact the steady-state cycling kinetics of the myosin heads engaging in contraction and can effectively induce a hypocontractile phenotype in treated cardiac muscle.

ACKNOWLEDGMENT The authors thank Mr Darron Marzolf who provided fresh farm pig hearts.

FUNDING SUPPORT AND AUTHOR DISCLOSURES

Research reported in this publication was supported by the National Heart, Lung, and Blood Institute of the National Institutes of Health under Award Numbers R01HL157169, R01HL171657, and R01HL128368; National Institute of Arthritis and Musculoskeletal and Skin Diseases of the National Institutes of Health under Award Number P30AR074990; and National Institute of General Medical Sciences under Award Number RM1GM131981. This project used resources from the University of Washington Center for Translational Muscle Research supported by National Institutes of Health grant P30AR074990. This research used resources of the Advanced Photon Source; a US Department of Energy (DOE) Office of Science User Facility operated for the DOE Office of Science by the Argonne National Laboratory under Contract DE-AC02-06CH11357. BioCAT is supported by National Institutes of Health grant P30 GM138395. The content is solely the responsibility of the

authors and does not necessarily represent the official views of the National Institutes of Health. This work was also supported by an American Heart Association Collaborative Sciences Award (to Dr Moussavi-Harami). Dr Mohran is a current employee of Kardigan Bio but completed this work before employment. Dr Ma consults for Edgewise Therapeutics, Cytokinetics Inc, and Kardigan Bio, but this activity has no relation to the current work. Dr Regnier is a consultant for Kardigan Bio and Bristol Myers Squibb; serves on the scientific advisory board for FilamenTech; and has equity in StemCardia, Inc and KineaBio, Inc; none of the current work is in conflict with these associations. All other authors have reported that they have no relationships relevant to the contents of this paper to disclose.

ADDRESS FOR CORRESPONDENCE: Dr Farid Moussavi-Harami, University of Washington, 850 Republican Street, D353, Seattle, Washington 98109, USA. E-mail: moussavi@uw.edu.

PERSPECTIVES

COMPETENCY IN MEDICAL KNOWLEDGE: The development and success of Afi in clinical trials provides a positive outlook for patients with HCM. Afi and Mava reduce cardiac contractility by different mechanisms of action, which opens the possibility for other small molecules that can also be effective in treating HCM.

TRANSLATIONAL OUTLOOK: It is expected that soon we will have 2 cardiac myosin inhibitors for treatment of obstructive HCM. Future studies could evaluate whether Mava and Afi effectiveness differs based on the HCM variant biophysical properties.

REFERENCES

1. Ommen SR, Ho CY, Asif IM, et al. 2024 AHA/ACC/AMSSM/HRS/PACES/SCMR guideline for the management of hypertrophic cardiomyopathy: a report of the American Heart Association/American College of Cardiology Joint Committee on Clinical Practice Guidelines. *J Am Coll Cardiol*. 2024;83(23):2324–2405.

2. Lopes LR, Ho CY, Elliott PM. Genetics of hypertrophic cardiomyopathy: established and emerging implications for clinical practice. *Eur Heart J*. 2024;45:2727–2734.

3. Olivotto I, Oreziak A, Barriales-Villa R, et al. mavacamten for treatment of symptomatic obstructive hypertrophic cardiomyopathy (EXPLORER-HCM): a randomised, double-blind, placebo-controlled, phase 3 trial. *Lancet*. 2020;396:759–769.

4. Heitner SB, Jacoby D, Lester SJ, et al. Mavacamten treatment for obstructive hypertrophic cardiomyopathy: a clinical trial. *Ann Intern Med*. 2019;170:741–748.

5. Green EM, Wakimoto H, Anderson RL, et al. A small-molecule inhibitor of sarcomere contractility suppresses hypertrophic cardiomyopathy in mice. *Science*. 2016;351:617–621.

6. Grillo MP, Erve JCL, Dick R, et al. In vitro and in vivo pharmacokinetic characterization of mavacamten, a first-in-class small molecule allosteric modulator of beta cardiac myosin. *Xenobiotica*. 2019;49:718–733.

7. Anderson RL, Trivedi DV, Sarkar SS, et al. Deciphering the super relaxed state of human beta-cardiac myosin and the mode of action of mavacamten from myosin molecules to muscle fibers. *Proc Natl Acad Sci U S A*. 2018;115:E8143–E8152.

8. Rohde JA, Roopnarine O, Thomas DD, Muretta JM. Mavacamten stabilizes an autoinhibited state of two-headed cardiac myosin. *Proc Natl Acad Sci U S A*. 2018;115:E7486–E7494.

9. Awinda PO, Bishaw Y, Watanabe M, Guglin MA, Campbell KS, Tanner BCW. Effects of mavacamten on Ca(2+) sensitivity of contraction as sarcomere length varied in human myocardium. *Br J Pharmacol*. 2020;177(24):5609–5621.

10. Scellini B, Piroddi N, Dente M, et al. Mavacamten has a differential impact on force generation in myofibrils from rabbit psoas and human cardiac muscle. *J Gen Physiol*. 2021;153(7):e202012789.

11. Maron MS, Masri A, Nassif ME, et al. Aficamten for symptomatic obstructive hypertrophic cardiomyopathy. *N Engl J Med*. 2024;390:1849–1861.

12. Hartman JJ, Hwee DT, Robert-Paganin J, et al. Aficamten is a small-molecule cardiac myosin inhibitor designed to treat hypertrophic cardiomyopathy. *Nat Cardiovasc Res*. 2024;3:1003–1016.

13. Kad NM, Wang H, Kennedy GG, Warshaw DM, Van Houten B. Collaborative dynamic DNA scanning by nucleotide excision repair proteins investigated by single- molecule imaging of quantum-dot-labeled proteins. *Mol Cell*. 2010;37:702–713.

14. Desai R, Geeves MA, Kad NM. Using fluorescent myosin to directly visualize cooperative activation of thin filaments. *J Bio Chem*. 2015;290:1915–1925.

15. Pilagov M, Naim A, Campbell KS, Kampourakis T, Geeves MA, Kad NM. Direct measurement of mavacamten and deoxyATP perturbation of the SRX/DRX ratio in porcine cardiac myofibrils using a simple, accessible and multiplexed approach. *J Muscle Res Cell Motil*. Published online October 22, 2025. https://doi.org/10.1007/s10974-025-09712-z

16. Kooiker KB, Mohran S, Turner KL, et al. Danicamtiv increases myosin recruitment and alters cross-bridge cycling in cardiac muscle. *Circ Res*. 2023;133:430–443.

17. Fischetti R, Stepanov S, Rosenbaum G, et al. The BioCAT undulator beamline 18ID: a facility for biological non-crystalline diffraction and X-ray absorption spectroscopy at the Advanced Photon Source. *J Synchrotron Radiat*. 2004;11:399–405.

18. Ma W, Gong H, Kiss B, Lee EJ, Granzier H, Irving T. Thick-filament extensibility in intact skeletal muscle. *Biophys J*. 2018;115:1580–1588.

19. Ma W, Henze M, Anderson RL, et al. The super-relaxed state and length dependent activation in porcine myocardium. *Circ Res*. 2021;129:617–630.

20. Powers JD, Kooiker KB, Mason AB, et al. Modulating the tension-time integral of the cardiac twitch prevents dilated cardiomyopathy in murine hearts. *JCI Insight*. 2020;5(20):e142446.

21. Tanner BC, Breithaupt JJ, Awinda PO. Myosin MgADP release rate decreases at longer sarcomere length to prolong myosin attachment time in skinned rat myocardium. *Am J Physiol Heart Circ Physiol*. 2015;309:H2087–H2097.

22. Turner KL, Morris HS, Awinda PO, Fitzsimons DP, Tanner BCW. RLC phosphorylation amplifies Ca2+ sensitivity of force in myocardium from cMyBP-C knockout mice. *J Gen Physiol*. 2023;155(4):e202213250.

23. Mulieri LA, Barnes W, Leavitt BJ, et al. Alterations of myocardial dynamic stiffness implicating abnormal crossbridge function in human mitral regurgitation heart failure. *Circ Res*. 2002;90:66–72.

24. Campbell KB, Chandra M, Kirkpatrick RD, Slinker BK, Hunter WC. Interpreting cardiac muscle force-length dynamics using a novel functional model. *Am J Physiol Heart Circ Physiol*. 2004;286:H1535–H1545.

25. Racca AW, Klaiman JM, Pioner JM, et al. Contractile properties of developing human fetal cardiac muscle. *J Physiol*. 2016;594:437–452.

26. Moussavi-Harami F, Razumova MV, Racca AW, Cheng Y, Stempien-Otero A, Regnier M. 2-Deoxy adenosine triphosphate improves contraction in human end-stage heart failure. *J Mol Cell Cardiol*. 2015;79:256–263.

27. Yang KC, Breitbart A, De Lange WJ, et al. Novel adult-onset systolic cardiomyopathy due to MYH7 E848G mutation in patient-derived induced

pluripotent stem cells. *JACC Basic Transl Sci*. 2018;3:728-740.

28. Leonard A, Bertero A, Powers JD, et al. Afterload promotes maturation of human induced pluripotent stem cell derived cardiomyocytes in engineered heart tissues. *J Mol Cell Cardiol*. 2018;118:147-158.

29. Hartman JJ, Hwee DT, Robert-Paganin J, et al. aficamten is a small-molecule cardiac myosin inhibitor designed to treat hypertrophic cardiomyopathy. *Nat Cardiovasc Res*. 2024;3(8):1003-1016.

30. Tesi C, Colomo F, Nencini S, Piroddi N, Poggesi C. Modulation by substrate concentration of maximal shortening velocity and isometric force in single myofibrils from frog and rabbit fast skeletal muscle. *J Physiol*. 1999;516(Pt 3):847-853.

31. Stehle R, Solzin J, Iorga B, Poggesi C. Insights into the kinetics of Ca2+-regulated contraction and relaxation from myofibril studies. *Pflügers Archiv - Eur J Physiol*. 2009;458:337-357.

32. Davis J, Davis LC, Correll RN, et al. A tension-based model distinguishes hypertrophic versus dilated cardiomyopathy. *Cell*. 2016;165:1147-1159.

33. Masri A, Cardoso RN, Abraham TP, et al. Effect of aficamten on cardiac structure and function in obstructive hypertrophic cardiomyopathy: SEQUOIA-HCM CMR Substudy. *J Am Coll Cardiol*. 2024;84:1806-1817.

34. Mohran S, Kooiker K, Mahoney-Schaefer M, et al. The biochemically defined super relaxed state of myosin—a paradox. *J Bio Chem*. 2024;300:105565.

35. Jani VP, Song T, Gao C, et al. The structural OFF and ON states of myosin can be decoupled from the biochemical super- and disordered-relaxed states. *PNAS Nexus*. 2024;3:pgae039.

36. Auguin D, Robert-Paganin J, Réty S, et al. Omecamtiv mecarbil and mavacamten target the same myosin pocket despite opposite effects in heart contraction. *Nat Commun*. 2024;15(1):4885.

37. Gollapudi SK, Ma W, Chakravarthy S, et al. Two classes of myosin inhibitors, para-nitroblebbistatin and mavacamten, stabilize beta-cardiac myosin in different structural and functional states. *J Mol Biol*. 2021;433:167295.

38. Kovács M, Tóth J, Hetényi C, Málnási-Csizmadia A, Sellers JR. Mechanism of blebbistatin inhibition of myosin II. *J Bio Chem*. 2004;279:35557-35563.

39. Zhao FQ, Padron R, Craig R. Blebbistatin stabilizes the helical order of myosin filaments by promoting the switch 2 closed state. *Biophys J*. 2008;95:3322-3329.

40. Ma W, Del Rio CL, Qi L, et al. Myosin in autoinhibited *off* state(s), stabilized by mavacamten, can be recruited in response to inotropic interventions. *Proc Natl Acad Sci U S A*. 2024;121(8):e2314914121.

41. Wheeler MT, Olivotto I, Elliott PM, et al. Effects of mavacamten on measures of cardiopulmonary exercise testing beyond peak oxygen consumption. *JAMA Cardiol*. 2023;8(3):240-247.

42. Ho CY, Mealiffe ME, Bach RG, et al. Evaluation of mavacamten in symptomatic patients with nonobstructive hypertrophic cardiomyopathy. *J Am Coll Cardiol*. 2020;75:2649-2660.

KEY WORDS cardiac myosin inhibitors, darcomere, engineered heart tissues, hypertrophic cardiomyopathy, muscle x-ray diffraction, myosin ATPase activity

APPENDIX For an expanded Methods section as well as supplemental figures and tables, please see the online version of this paper.